



# Matrix metalloproteinase 9-activatable peptide-conjugated hydrogel-based fluorogenic intraocular-lens sensor

Moo-Kwang Shin<sup>a,1</sup>, Yong Woo Ji<sup>b,c,1</sup>, Chae-Eun Moon<sup>b</sup>, Hyo Lee<sup>a</sup>, Byunghoon Kang<sup>a</sup>, Woo-Seok Jinn<sup>a</sup>, Jisun Ki<sup>a</sup>, Byunggeol Mun<sup>a</sup>, Myeong-Hoon Kim<sup>a</sup>, Hyung Keun Lee<sup>b,d,e,\*\*</sup>, Seungjoo Haam<sup>a,\*</sup>

<sup>a</sup> Department of Chemical & Biomolecular Engineering, College of Engineering, Yonsei University, 50 Yonsei-ro, Seodaemun-gu, Seoul, 03722, Republic of Korea

<sup>b</sup> Institute of Vision Research, Department of Ophthalmology, Yonsei University College of Medicine, 50-1 Yonsei-ro, Seodaemun-gu, Seoul, 03722, Republic of Korea

<sup>c</sup> Department of Ophthalmology, National Health Insurance Service Ilsan Hospital, 100 Ilsan-ro, Ilsandong-gu, Goyang, 10444, Republic of Korea

<sup>d</sup> Institute of Vascular Disease and Metabolism, Yonsei University College of Medicine, 50-1 Yonsei-ro, Seodaemun-gu, Seoul, 03722, Republic of Korea

<sup>e</sup> College of Pharmacy, Yonsei University, 85 Songdogwahak-ro, Yeonsu-gu, Incheon, 21983, Republic of Korea

## ARTICLE INFO

### Keywords:

Intraocular-lens sensor  
Hydrogel sensor  
Peptide-probe  
Matrix metalloproteinase-9  
Liquid biopsy

## ABSTRACT

The eye is an extension of the central nervous system (CNS) and contains aqueous humor (AH), which is a fluid rich in biomolecules secreted from intraocular tissues; thus, this organ allows for non-invasive visualization of early changes in CNS disorders. There is a growing interest in developing implantable devices, such as intraocular-lens (IOL), for specific medical uses, including intraocular monitoring. We describe a novel IOL-sensing system for detecting AH biomarkers via biocompatible enzyme-activatable fluorogenic hydrogel sensors. Matrix-metalloproteinase-9, a biomarker of degenerative CNS and eye disorders, was selected as a target. A peptide-probe-incorporated fluorogenic IOL (FIOL) was developed using diacrylamide-group-modified poly (ethyleneglycol) (PEGDAAm) biocompatible hydrogels, adjusting the hydrogel mesh size to allow selective penetration of the target while blocking non-targets, using label-free detection with semi-permanently implantable sensors, and demonstrating the clinical feasibility of FIOL through *in vivo* testing. This novel FIOL-based sensing system represents a promising approach for liquid biopsy of intraocular fluids.

## 1. Introduction

The eye is richly innervated by the central nervous system (CNS) and shares the same vascular supply (Deghani et al., 2018; Lim et al., 2016; London et al., 2013). The retina, as the inner tissue of the eye, is a developmental outgrowth of the brain. It is well known that the optic nerve is the second cranial nerve and carries sensory information toward the visual centers in the brain. Particularly, the intraocular aqueous humor (AH) contains endogenous biomolecules secreted from these intraocular neural tissues as it circulates inside the eye all the time (Hillier et al., 2017; Inoue et al., 2013; Janciauskiene et al., 2011; Jonas et al., 2012; Kang et al., 2014; Midena et al., 2020; Pietrowska et al., 2018). Therefore, the eye allows for non-invasive visualization of pathologic changes in CNS disorders, such as multiple sclerosis,

Parkinson's disease, and Alzheimer's disease (Boerger et al., 2019; Ekker et al., 2017; Green et al., 2010; Janciauskiene et al., 2011; London et al., 2013; van Wijngaarden et al., 2017) beyond eye diseases (Hillier et al., 2017; Kersten et al., 2018; Lambert et al., 2016; Tezel, 2013).

The intraocular-lens (IOL) is a device implanted into the ocular chambers filled with AH as an essential part of treatment for cataracts or presbyopia (Kohnen, 2018; Li and Jie, 2019). Its implantation has become the most frequently performed ocular procedure worldwide (Busbee et al., 2002; Park et al., 2016). Owing to recent advances in biosensing technology, there is a growing interest in the development of intraocular devices, including IOL, for specific medical uses such as intraocular monitoring (Araci et al., 2014; Narasimhan et al., 2018; Yang et al., 2018). It has been demonstrated that novel intraocular sensors on an implantable device can continuously monitor changes in

\* Corresponding author.

\*\* Corresponding author. Institute of Vision Research, Department of Ophthalmology, Yonsei University College of Medicine, 50-1 Yonsei-ro, Seodaemun-gu, Seoul, 03722, Republic of Korea.

E-mail addresses: [shadik@yuhs.ac](mailto:shadik@yuhs.ac) (H.K. Lee), [haam@yonsei.ac.kr](mailto:haam@yonsei.ac.kr) (S. Haam).

<sup>1</sup> These authors contributed equally to this work.

glucose concentration or intraocular pressure (IOP) (Araci et al., 2014; Lee et al., 2017; Narasimhan et al., 2018; Yang et al., 2018). Monitoring pathological changes is necessary to target disease-specific biomolecules such as proteins for early diagnosis (Fuentes-Arderiu, 2013); however, IOL-based macromolecular proteinic biomarker-sensing platforms have not yet been developed.

Hydrogels (i.e., poly(2-hydroxyethyl methacrylate) (PHEMA), poly(ethyleneglycol) (PEG) hydrogels) are practical candidates for use in IOL-based sensing devices as they are already successfully used in implantation because of their high biocompatibility (Angelova and Hunkeler, 1999; Drury and Mooney, 2003; Hoffman, 2002; Wahid Khan et al., 2014). PEG hydrogels are particularly important because of their antifouling and anti-adsorptive properties regarding non-specific proteins (Banerjee et al., 2011). Additionally, diacrylamide-group-modified PEG diacrylamide (PEGDAAm) hydrogels are more stable than the currently used PEG diacrylate (PEGDA) hydrogels. Moreover, hydrogels can be easily modified with label-free sensing probes, including enzyme-degradable peptides (Benton et al., 2009; Seo et al., 2015; Ulijn et al., 2007). Therefore, sensing probe-conjugated PEG hydrogels would enable non-invasive and long-term label-free disease monitoring of the AH inside the eye using IOL-based sensing devices.

In the present study, we described a novel IOL-based sensing system for detecting AH biomarkers via a biocompatible enzyme-activatable fluorogenic hydrogel sensor. As a proof of concept, matrix metalloproteinase (MMP)-9 was selected as a target in AH because it is one of the biomarkers of CNS and eye disorders (Tamhane et al., 2019; Vafadari et al., 2016). First, MMP-9-responsive fluorogenic PEGDAAm hydrogel sensors were developed by conjugating specifically cleavable fluorogenic peptide-probes with MMP-9. Next, a fluorogenic hydrogel sensor attached to an IOL sensor (FIOL) was developed. Finally, to prove the clinical feasibility of the FIOL *in vivo*, we implanted our novel FIOL in rabbits via cataract surgery and monitored changes in the fluorescence signal in association with increasing intraocular MMP-9 concentrations. This newly developed sensing system offers a promising approach for IOL-based liquid biopsy (LB) using intraocular fluids as clinical specimens.

## 2. Materials and methods

### 2.1. Synthesis of PEGDAAm precursor

PEGDAAm was synthesized according to a method adapted from Elbert et al. (Elbert and Hubbell, 2001) and Cosgriff-Hernandez et al. (Browning et al., 2014). To synthesize PEGDAAm, we modified the end group of PEG diamine. Briefly, 61.8 g of PEG diamine was dissolved in 75 mL of DCM. After the solution became transparent, 7 mL of DIPEA was injected, followed by a dropwise injection of 6.66 mL of acryloyl chloride at 4 °C with vigorous stirring. The reaction was conducted overnight under nitrogen with refluxing and protection from light. The reactant was filtered and precipitated in 1 L of diethyl ether. The obtained PEGDAAm powder was then vacuum-dried. To eliminate by-products, the obtained powder was dissolved in 200 mL of 1 M K<sub>2</sub>CO<sub>3</sub> solution for 6 h, followed by DCM extraction. The concentrated solution was precipitated in 1 L of diethyl ether twice and then vacuum-dried.

### 2.2. PEGDAAm hydrogel fabrication and stability

PEGDAAm and PEGDA hydrogels were prepared using the photopolymerization method. Briefly, aqueous solutions of PEGDAAm or PEGDA (20 wt %) with 0.1% (w/v) HMPP were photo-polymerized in a 48-well plate (flat clear-bottom) using an 8-W UV lamp (LF-104.L, UVITEC, Cambridge, UK) (365 nm, 120 s) at a distance of 1 cm. The fabricated hydrogels were dispersed in 5 mL of various solutions: 0.1 M HCl, 0.1 M NaOH, PBS, Balanced salt solution (BSS), and DW. The stability of PEGDAAm and PEGDA hydrogels was analyzed by weekly measurements of the mass.

### 2.3. Cell viability test

The cornea endothelial cell line, BCE C/D1b, denoted as CECs, was obtained from ATCC (Manassas, VA, USA) and cultured in complete growth medium containing 10% fetal bovine serum, human corneal growth supplement, and 1% antibiotic-antimycotic (Gibco®, Grand Island, NY, USA). The cytotoxicity of PEGDAAm against cornea endothelial cells (CECs) was evaluated by measuring cell growth using the MTT assay. CECs ( $1 \times 10^4$  cells/well) were seeded in a 96-well plate and incubated at 37 °C under 5% CO<sub>2</sub> for 24 h. After removing the culture medium, cells were treated with 100 µL of complete growth medium, containing i) 10-fold serial dilutions of PEGDAAm solution ( $50 \times 10^{-5} \times 10^{-8}$  mM) or ii) the supernatant of PEGDAAm hydrogel dispersed in the media for 1, 3, 5, and 7 days and incubated for 24 h. Subsequently, the culture medium was replaced with 0.5 mg/mL MTT solution (Thermo Fisher Scientific, Waltham, MA, USA) diluted in serum-free media and incubated for 2 h at 37 °C. The cells were washed with DPBS, treated with 50 µL of MTT solution, and then incubated for another 2 h. The MTT solution was removed, and 100 µL DMSO was added to each well. The plates were then shaken for 30 min to dissolve the remaining crystals completely. The optical density (O.D.) was measured at 570 nm.

### 2.4. Protein diffusion test

Synthesized hydrogels were dispersed in 100 µL of standard protein marker (10–250 kDa recombinant proteins) for 12 h. Supernatant protein markers were removed, the remaining hydrogels were rinsed with 100 µL PBS, and then re-dispersed in 50 µL PBS for 12 h. The supernatants were collected, and the proteins inside the different mesh-sized hydrogels were analyzed by SDS-PAGE.

### 2.5. Conjugation of peptide-probes inside the hydrogel (method (ii))

For the conjugation of the peptide-probe, amino group-modified PEGDAAm-co-PAA hydrogels were fabricated. Specifically, 4.5 wt % of PEGDAAm and 0.5 wt % of allylamine were polymerized for 5 min with 0.5% of photoinitiator. Next, 8 µmol of peptide-probes (20 mM) was pre-activated by shaking with 80 µmol of EDC (30 µg/µL DMSO) for 5 min, followed by the addition of 40 µmol of sulfo-NHS (40 µg/µL DMSO) with 8 µmol of TEA; subsequently, this was shaken for an additional 5 min. Pre-activated peptide-probes with EDC/sulfo-NHS were added to the surface of PEGDAAm-co-PAA hydrogels and agitated for 3 h. Extensive dialysis was performed using DPBS, ethanol, and reaction buffer.

### 2.6. Hydrogel sensor reaction with MMP-9

Using peptide-probes and hydrogel sensors for MMP-9, the fluorescence signal for serially diluted MMP-9 was measured, and the limit-of-detection (LOD) was calculated. To evaluate selectivity, we compared this fluorescence signal to those of MMP-3, MMP-9, and BACE1 (Enzo Life Sciences, NY, USA). Before the reaction, peptide-probes, hydrogel sensors, and enzymes were dispersed in reaction buffer (50 mM Tris, 150 mM NaCl, 5 mM CaCl<sub>2</sub>, and 0.025% Brij35, pH 7.5) followed by pre-activation at 37 °C for 1 h. For the LOD test of the probe, 20 nmol of peptide-probe and allyl-peptide-probe (dispersed in 100 µL buffer) were reacted with 100 µL of MMP-9 (0 to 20 nM). For the LOD test of the PEGDAAm-co-PAA hydrogel sensor, 80 µL volume of hydrogel sensor was prepared by the conjugation of 40 nmol of peptide-probe using EDC/NHS chemistry. After the dialysis of the hydrogel sensor, the sensor was reacted with 100 µL of MMP-9 (0 to 20 nM). For the selectivity test of the hydrogel sensor, the fluorescence was measured after the reaction of MMP-9 and 5x MMP-3 and BACE1. All fabrication and signal tests were conducted under protection from light.

## 2.7. Development of FIOl

To prepare the PHEMA IOL supports, the 3D printed IOL mold was fabricated with an SLA 3D printer (Form2, formlabs, MA, USA). The IOL mold was designed by computer-aided design (CAD) (TINKERCADTM, Autodesk, Inc., San Rafael, CA, USA). The 3D-printed IOL mold was transferred into a PDMS mold (silicon elastomer base: curing agent = 10:1, 45 °C for 1 day). To prepare the PHEMA IOL supports, 30  $\mu$ L PHEMA hydrogel (90 wt % composed of PHEMA and EGDMA), containing 1 wt % of PI, was polymerized under UV light for 3 min inside the IOL mold. The PHEMA IOL was ejected from the mold and dispersed in excess DPBS to remove unreacted monomers. A volume of 6  $\mu$ L PEGDAAm-co-PAA hydrogel (5 wt %) was added to the inside of the channel of the IOL supports. After removing the free monomers by washing with DPBS, 10  $\mu$ L peptide-probe activated by EDC/sulfo-NHS was added to the PEGDAAm-co-PAA hydrogel in the channel and reacted for 3 h in the dark. The resulting hydrogel sensor was attached to IOL to complete the FIOl. Then, it was dialyzed using ethanol, DPBS, and reaction buffer.

## 2.8. FIOl in vivo implantation via cataract surgery

Animal experiments were performed in accordance with the standards outlined in the Association for Research in Vision and Ophthalmology Statement for the Use of Animals in Ophthalmic and Vision Research. The research protocol was approved by the Institutional Animal Care and Use Committee of the Yonsei University College of Medicine. New Zealand white rabbits (DooYeol Biotech, Seoul, Korea) (33 weeks old, 2 kg, male) were used for this study. Their eyes were examined under the slit-lamp before the surgery and found to be unremarkable. The surgical procedure of FIOl implantation was performed by a single experienced surgeon (Y. W. J) using conventional cataract surgery. Briefly, rabbits were anesthetized before surgery (30 mg/kg of zoletil 50 Inj., Virbac Korea, Seoul, Korea). A paracentesis incision was created at the 2 o'clock area of the peripheral cornea; viscoelastic (Healon, Alcon, Fort Worth, Texas, USA) was injected into the anterior chamber, and a superotemporal clear cornea incision was created using a 2.75-mm keratome blade. Continuous curvilinear capsulorhexis was performed manually, followed by phacoemulsification with Millennium Microsurgical System (Bausch & Lomb Inc., Rochester, NY, USA) using a divide and conquer technique for lens nucleus, irrigation and aspiration of cortical remnants, FIOl implantation into the intact capsular bag, and evacuation of the viscoelastic. Post-operative antibiotic and steroid eye drops were given three times a day for 2 weeks.

## 2.9. MMP-9 detection using FIOl

The fluorescence of FIOl after reaction with MMP-9 (0–20 nM) was evaluated. Specifically, FIOl was placed in a 48-well plate and pre-activated with 200  $\mu$ L of reaction buffer for 1 h at 37 °C. Each concentration of MMP-9 was pre-activated under the same conditions. Next, 100  $\mu$ L MMP-9 was added to each well and reacted for 2.5 days. For MMP-9 sensing of FIOl inside *in vivo* rabbit eyes, 100  $\mu$ L of MMP-9 (100 nM) was injected into the anterior chamber through the corneal paracentesis using a 30-gauge syringe. The injection was repeated five times, and the change in FIOl fluorescence was observed with a slit-lamp under cobalt blue-filtered light.

## 2.10. Statistical analysis

Continuous variables were examined for normal distribution by the Kolmogorov-Smirnov test. For variables that deviated from a normal distribution, Student *t*-test and one-way analysis of variance (ANOVA) were used for comparisons between two samples and among three or more groups, respectively. Bonferroni-corrected Dunnett's procedure was used as a post-doc analysis. Statistical analysis was performed using SAS (ver. 9.13; SAS, Cary, NC) and R (ver. 3.2.5; Statistics and

Mathematics, Vienna, Austria). Results are presented as the mean  $\pm$  standard deviation. P-values < 0.05 were considered significant.

## 3. Results and discussion

### 3.1. Synthesis and characteristics of PEGDAAm hydrogel

PEGDAAm hydrogel was used to develop a biocompatible and bio-stable hydrogel sensor. PEGDAAm was synthesized from a PEG3k diol as described previously (Browning et al., 2014; Elbert and Hubbell, 2001), with modifications (Fig. 1a). Chemical structures of the synthesized polymer were analyzed by Fourier transform IR (FT-IR) and  $^1$ H NMR spectroscopy. Step-by-step FT-IR spectra were obtained during PEGDAAm synthesis (Fig. 1b). A stretch vibration peak for S–O in mesylate appeared at approximately 800–725  $\text{cm}^{-1}$ . After the PEG diamine was formed, absorption peaks appeared at 3432, 1654, and 1575  $\text{cm}^{-1}$ , corresponding to one N–H stretch vibration and two bending vibrations, respectively. The disappearance of N–H peaks and the appearance of C=O stretch (1667 and 1624  $\text{cm}^{-1}$ ) and N–H bending (1543  $\text{cm}^{-1}$ ) peaks for the amide bond indicated successful synthesis of PEGDAAm (Browning et al., 2014; Browning and Cosgriff-Hernandez, 2012; Elbert and Hubbell, 2001). Synthesized polymers were also confirmed by  $^1$ H NMR spectroscopy (Fig. S1) (Mahou and Wandrey, 2012; Stevens et al., 2015).

To confirm the enhanced stability of PEGDAAm hydrogels, PEGDAAm and PEGDA hydrogels (20 wt %, 200  $\mu$ L each) were dispersed in acidic (0.1 M HCl) and basic (0.1 M NaOH) solutions for several weeks. The prepared PEGDA hydrogel was completely dissolved within 3 h of dispersion in 0.1 M NaOH (Fig. 1c) and within 1 week in 0.1 M HCl (Fig. 1d). However, the PEGDAAm hydrogel maintained its stability owing to its chemically stable amide bond compared to the ester bond of PEGDA, which is prone to hydrolysis. Additionally, PEGDAAm was found to be stable in the intraocular system. BSS, used as irrigating fluid during intraocular surgery clinically, has a composition similar to AH. No differences in weight change were observed for PEGDAAm hydrogels in BSS, DW, and DPBS (Fig. 1e). Besides, the compression strength of the PEGDAAm hydrogel was evaluated using a universal testing machine (UTM). The compressive stress (at 70% strain) of 5, 10, and 20 wt% PEGDAAm hydrogel was 1.1, 8.1, and 21.2  $\text{kPa}/\text{mm}^2$ , respectively. Under equal stress (3  $\text{kPa}/\text{mm}^2$ ), the 5 wt% PEGDAAm hydrogel could endure over 80% deformation, whereas the 10 and 20 wt% PEGDAAm hydrogel showed 2.7 and 1.9% deformation (Fig. S2). Considering that FIOl would be folded inside the injector to be inserted into the posterior chamber during surgery, a highly deformable hydrogel would be beneficial for implantation.

The *in vitro* cytotoxicity of PEGDAAm was evaluated using CECs. Ten-fold serial dilutions of the PEGDAAm monomer, (50 mM to 5 nM), were used to treat CECs. The PEGDAAm monomer showed no cytotoxicity below 50 mM (Fig. 1f). Also, unreacted or degraded PEGDAAm monomer was present in the hydrogels, indicating that the determination of the cumulative concentration of PEGDAAm eluted from prepared hydrogels is essential. To evaluate this parameter, 20 wt % PEGDAAm hydrogels were dispersed in  $\text{D}_2\text{O}$ , followed by an analysis of the supernatant solutions by  $^1$ H NMR. The saturated cumulative PEGDAAm eluted concentration was approximately 273.65  $\mu\text{M}$  according to the standard  $^1$ H NMR curve of the PEGDAAm monomer (Fig. 1g). *In vitro* cell viability test showed that there was no toxicity to CECs. Thus, we anticipated that the cumulatively eluted PEGDAAm would have no adverse effect on cell viability *in vivo*. Additionally, because the prepared PEGDAAm hydrogels were not dialyzed and washed during this test, PEGDAAm should not be detectable after an excessive dialysis procedure (Fig. 1h). Therefore, these biostable and biocompatible PEGDAAm hydrogel were deemed to be adequate for hydrogel-sensing materials.

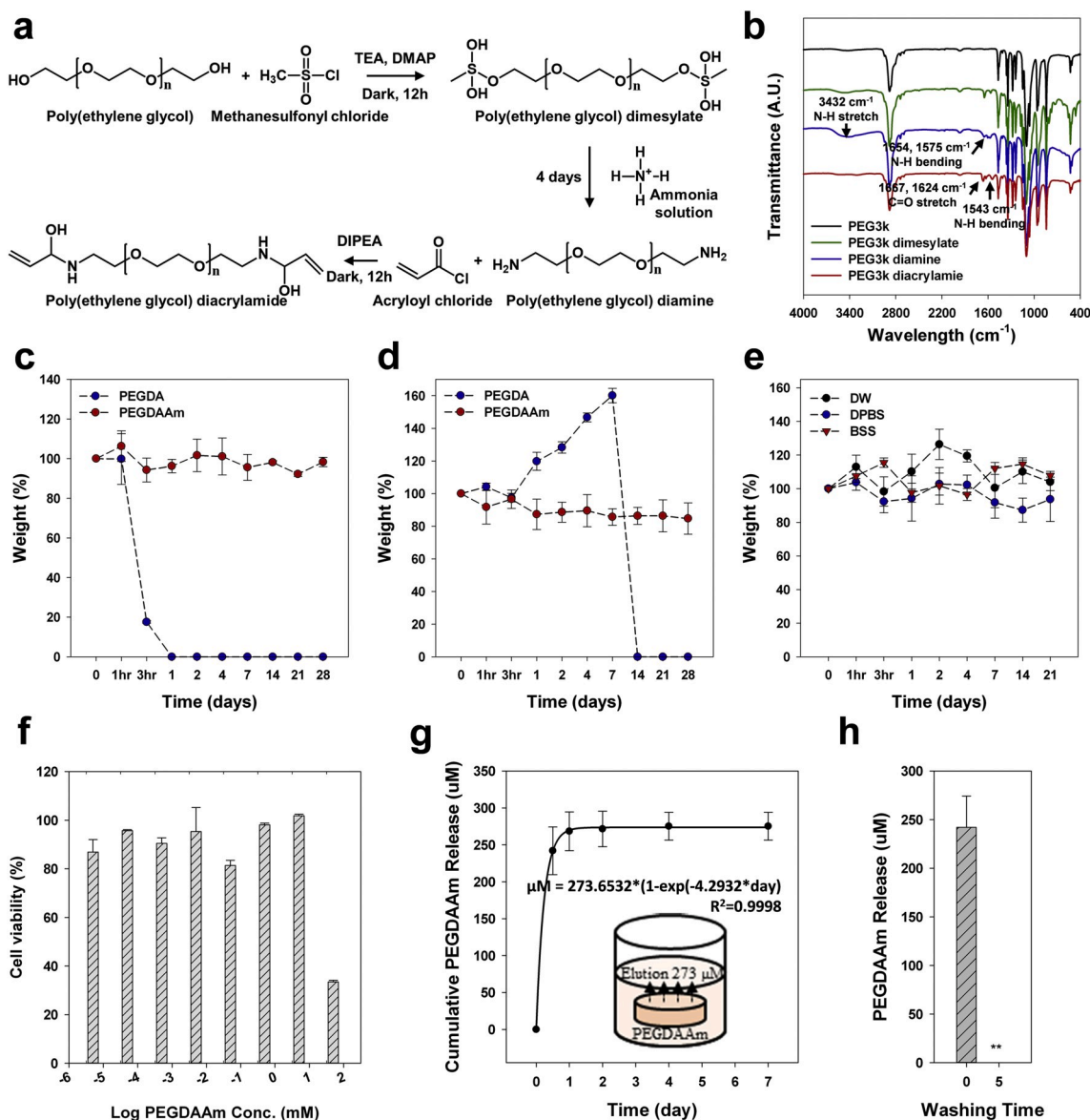


**Fig. 1.** Synthesis and characteristics of PEGDAAm hydrogel. (a) Schematic illustration of PEGDAAm synthesis. PEGDAAm was prepared from PEG diamine by introducing an acryloyl group at each end. (b) FT-IR spectra of PEG diol, PEG dimesylate, PEG diamine, and PEGDAAm. C=O (1667, 1624 cm<sup>-1</sup>) and N-H (1543 cm<sup>-1</sup>) representative peaks of the amide bond in PEGDAAm indicated the complete-synthesis of the polymer. Mass change graphs of PEGDA and PEGDAAm hydrogels dispersed in solutions containing (c) 0.1 M NaOH, (d) 0.1 M HCl, and (e) BSS. (f) PEGDAAm polymer cytotoxicity (*in vitro*) in CECs according to concentration (0–50 mM serial dilution). (g) PEGDAAm hydrogel was dispersed, and the supernatants were collected at 0-, 0.5-, 1-, 2-, 4-, and 7 days. Each collected supernatant was analyzed using <sup>1</sup>H NMR spectroscopy, and the cumulative eluted PEGDAAm concentration from the hydrogel was plotted by a linear regression standard curve. (h) Eluted concentrations of PEGDAAm with and without washing five times. (\*\*: not detectable).

### 3.2. Development of MMP-9 responsive hydrogel sensor

To develop a novel intraocular MMP-9-responsive hydrogel sensor, a fluorogenic peptide-probe specifically cleavable by MMP-9 was conjugated inside the PEGDAAm hydrogel. As intraocular-based sensors are implanted semi-permanently, a label-free sensing system is needed to minimize additional invasive surgical procedures. For label-free detection, a fluorescence reporter (5-FAM; Ex/Em = 492/518 nm) and quencher (dabcyl, Ab. ~450 nm), were conjugated to the end of the peptide-probe for use in fluorescence resonance energy transfer (FRET). Because the implanted hydrogel sensor should be analyzed inside the eye by external fluorescence measuring devices, it would be beneficial to use visible light with a longer wavelength to minimize side effects to the eye. The sequence “GPQG↓↓IAGQ” originated from the collagen alpha-1 chain was effectively cleaved by MMP-9 through its collagenase activity

(Fields et al., 1990). Consequently, the sequence of 5-FAM-GPQ-GIAGQLK (dabcyl) was selected as a fluorogenic peptide-probe (Fig. S3, Table S1). Based on the proteolytic activity of MMP-9, the fluorogenic peptide-probe in its FRET-OFF state was selectively cleaved by MMP-9, changing to the FRET-ON state and showing an increased fluorescence signal (Fig. 2a).

The carboxyl group-terminated peptide-probe was incorporated into the hydrogel based on the EDC/NHS chemistry present during hydrogel sensor fabrication. To include a site that could form an amide bond between the peptide-probe and the side chain of the hydrogel, a PEGDAAm-co-poly(allylamine) (PEGDAAm-co-PAA) hydrogel was prepared. The C-terminus of the peptide-probe was conjugated to the primary amine of the PEGDAAm-co-PAA hydrogel. Two similar methods were used to conjugate the peptide-probe inside the hydrogel. Method (i) introduced a vinyl group at the C-terminus of the peptide-probe

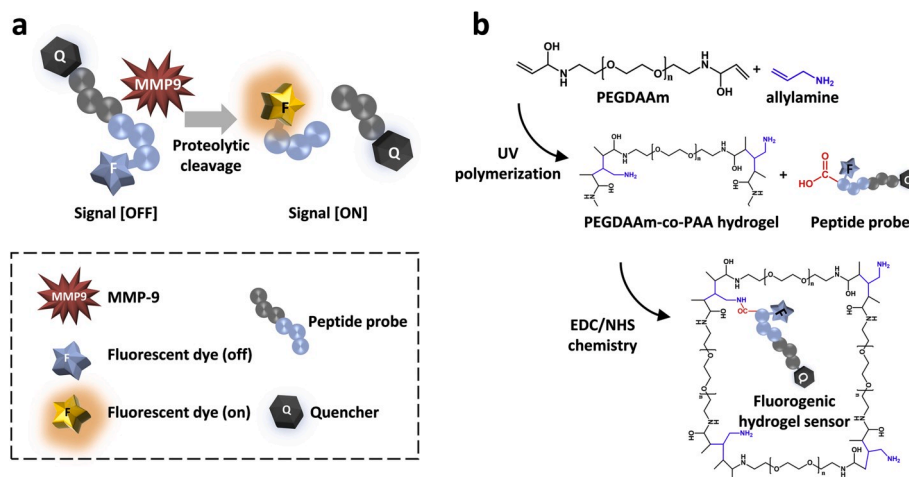


**Fig. 2.** Development of MMP-9 responsive hydrogel sensor. Schematic illustration of the (a) sensing mechanism of FRET-based peptide-probes and (b) probe conjugation *Method (ii)*. Copolymerization of PEGDAAm and allylamine under UV irradiation, followed by conjugation of the peptide-probe at the side chain of the amine using EDC/NHS chemistry to obtain the PEGDAAm-co-allyl-peptide-probe hydrogel sensor.

followed by copolymerization with hydrogel monomers (Fig. S4); *Method (ii)* involved the fabrication of a primary amine group-modified with hydrogel, followed by peptide-probe conjugation with the primary amine inside the hydrogel (Fig. 2b). However, for the hydrogel sensor prepared by *Method (i)*, no increase in fluorescent signal was observed (Fig. S5). During polymerization for the hydrogel, the radicals produced by a photoinitiator (PI) with UV or APS with TEMED affected the C=C

double bond with the fluorescent dye, which induced a structural breakdown and altered the fluorescent properties of the dye (Fig. S6). In contrast, the hydrogel sensor prepared using *Method (ii)* showed reactivity to MMP-9 (if the EDC/NHS reaction was conducted under PBS instead of DMSO, no signal was observed, Fig. S7); thus, *Method (ii)* was used to fabricate the peptide-probe-conjugated PEGDAAm hydrogel sensor.

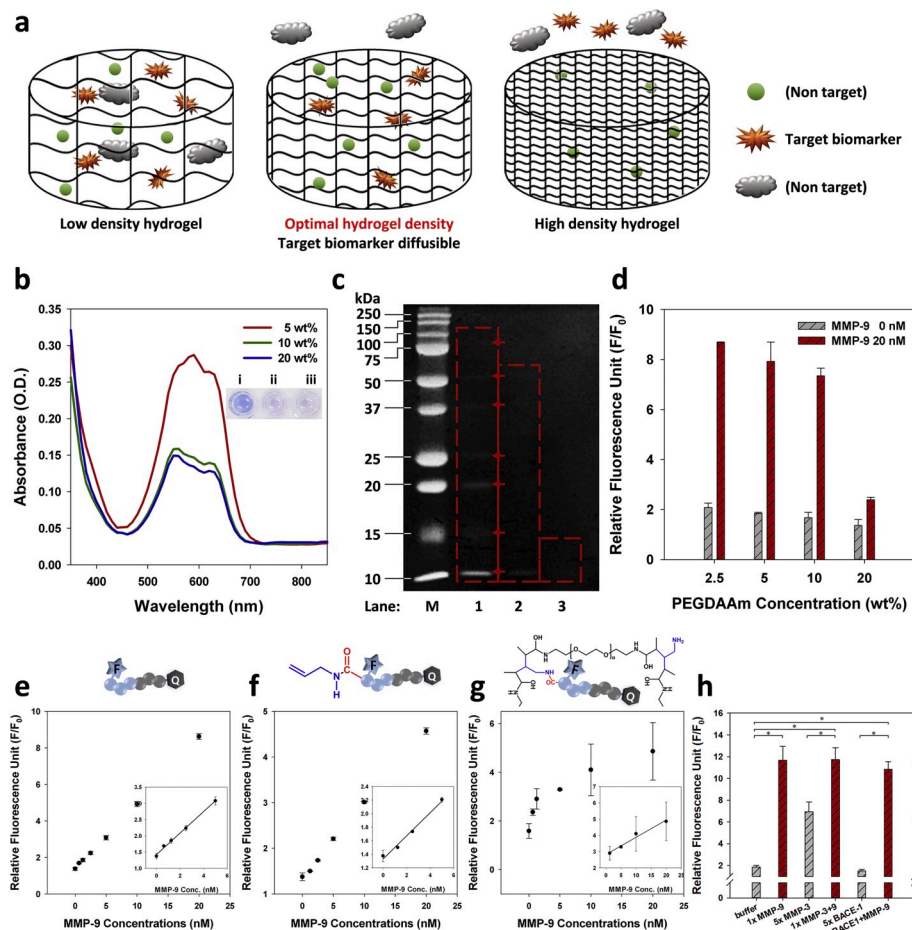


**Fig. 3.** MMP-9 detection using the PEGDAAm hydrogel sensor. (a) Schematic illustration of selective protein diffusion inside the hydrogel via the adjustment of the cross-linking density. (b) Absorbance spectra of the (i) 5, (ii) 10, and (iii) 20 wt % PEGDAAm hydrogels after protein marker diffusion. (c) SDS-PAGE analysis of the proteins diffused from the hydrogel. Lane M contains the molecular weight marker; lanes 1–3 contain supernatants of eluted protein markers from 5, 10, and 20 wt % hydrogels, respectively. (d) Fluorescence change in hydrogel sensors of different PEGDAAm densities after reaction with MMP-9 (20 nM). LOD calculation of (e) free-peptide-probe, (f) allyl-peptide-probe, and (g) peptide-probe-conjugated PEGDAAm-co-PAA hydrogels. LOD was calculated by linear regression of the curve (inset). (h) Hydrogel sensor selectivity with MMPs (MMP-3 and -9) and BACE1.  $*P < 0.001$ .

### 3.3. Optimization of the hydrogel mesh size

Hydrogel mesh size is vital for specific biomarker detection because efficient diffusion of a target biomarker into the hydrogel allows for reliable sensor activation. High-molecular-weight proteins cannot effectively diffuse into a highly cross-linked hydrogel; thus, appropriate control of the cross-linking density of the hydrogel sensor based on the molecular weight of the target biomarker is necessary (Fig. 3a). To investigate protein diffusivity through the PEGDAAm hydrogel, the hydrogel density was adjusted from 5 to 20 wt % of the total hydrogel mass. Prepared hydrogels were dispersed in 100  $\mu$ L protein marker solutions (10–250 kDa). After thoroughly soaking to diffuse the proteins into the hydrogels, excessive protein markers in the supernatant were removed. Color differences were directly observed between the 5 versus 10 and 20 wt % hydrogels (inset image of Fig. 3b). The absorbance of the samples was also analyzed with a microplate reader; protein markers had absorbance wavelengths of 550–650 nm and the highest O.D. was observed at 5 wt % PEGDAAm hydrogel (Fig. 3b), indicating that more proteins diffused into the least dense hydrogels.

Protein diffusivities were also analyzed by sodium dodecyl sulfate (SDS)-PAGE. Hydrogels were re-dispersed in 50  $\mu$ L of DPBS, and the proteins that had previously been soaked inside the hydrogel were diffused out. Supernatants were collected and analyzed by SDS-PAGE. Proteins with molecular weights ranging from 10 to 100 kDa diffused inside the 5 wt % PEGDAAm hydrogels, whereas only 10–50 and 10–15 kDa proteins diffused inside the 10 and 20 wt % PEGDAAm hydrogels, respectively (Fig. 3c). As described above, a high density of cross-linkers generated hydrogels with a smaller mesh size (Fig. S8).

To determine the relationship between protein diffusivity and hydrogel sensor activation, hydrogel sensors fabricated with different PEGDAAm densities (2.5, 5, 10, and 20 wt %) were used. Considering the 39-kDa MMP-9 catalytic domain as a target biomarker, MMP-9 diffused into hydrogels with a density lower than 10 wt % based on SDS-PAGE analysis. Interestingly, hydrogel sensors with densities of 2.5, 5, and 10 wt % showed increased fluorescence signals after reaction with 20 nM of MMP-9 (Fig. 3d). These results are consistent with those of hydrogel activity toward MMP-9, demonstrating that the molecular cut-off values of the hydrogel sensor can be adjusted to prevent non-specific biomolecule diffusion, allowing enzymatic activities of target biomarkers to occur inside the hydrogel sensor. Thus, the PEGDAAm hydrogel density was optimized to 5 wt % to enable sufficient diffusion of MMP-9 for cleavage of the peptide-probe.

### 3.4. MMP-9 detection using PEGDAAm hydrogel sensor

To assess the performance of the MMP-9 hydrogel sensor, its LOD and selectivity were analyzed. First, the LODs of the peptide-probe, allyl-peptide-probe, and PEGDAAm-co-PAA hydrogel sensor were measured using two-fold serial dilutions of MMP-9 (0–20 nM). The LOD of the peptide-probe, allyl-peptide-probe, and PEGDAAm-co-PAA hydrogel sensor were 262.76 pM, 675.26 pM, and 4.02 nM, respectively (Fig. 3e–g). The LOD was observed to decrease at each step of hydrogel sensor fabrication. Because the C-terminus of the probes was conjugated with the hydrogel side chain, steric hindrances increased probe access to the catalytic domain of the enzymes, which decreased the sensitivity. However, the decreased sensitivity should not affect the sensor performance as intraocular hydrogel sensors are intended to be implanted semi-permanently, and the biomarker in the AH cumulatively affects the hydrogel sensor. Finally, the selectivity of the PEGDAAm-co-PAA hydrogel sensor was investigated using MMPs (MMP-3 and -9) and BACE1 (beta-amyloid cleaving enzyme 1, which is involved in Alzheimer's diseases). The hydrogel sensor showed dramatically increased fluorescence signals in the presence of MMP-9, as expected (Fig. 3h, Fig. S9). Thus, the fluorogenic peptide-probe-conjugated PEGDAAm-co-PAA hydrogel MMP-9 sensor showed specific reactivity for MMP-9 with a LOD of 4.02 nM.

### 3.5. Development of FIOl

For the preparation of IOL-based sensing devices, 3D-blueprints can be designed to make holes or channels in the IOL surface to attach hydrogel sensors. While the IOL comprises optic and haptic parts, only the center of the optic part contributes to the patient's eyesight; thus, the modification of the entire haptic or the periphery of the optic is possible without sight interruption (Fig. S10a). However, the attachment of the hydrogel sensor onto the haptic may require compulsory pupil-dilation because the haptic is inserted behind the pupil to physically support IOL positioning. Therefore, the optimal location to attach a hydrogel sensor to the IOL is the periphery of the optic (Fig. S10b).

A fluorogenic hydrogel sensor-attached IOL sensor (FIOl) was prepared to determine whether hydrogel sensors are activatable *in vivo*. First, the IOL with round channels at the edge of the optic was fabricated by stereolithography (SLA) 3D printing and polydimethylsiloxane (PDMS) casting (Fig. 4a(i)–(ii)). Hydrophilic and acrylic PHEMA was used as the IOL material, which is currently FDA-approved for IOL implantation. Specifically, 90 wt % of a PHEMA precursor solution was polymerized on the PDMS IOL mold, followed by removal from the mold (Fig. 4a(iii)–(iv)). Single-, dual-, and triple-channeled IOLs were made (Fig. 4b). Subsequently, the PEGDAAm-co-PAA hydrogel sensor was embedded onto the channel of the PHEMA IOL (Fig. 4a(v)). PEGDAAm-co-PAA hydrogels developed on the channel provided specific conjugation sites for peptide-probes (Fig. 4a(vi)). After conjugation of the peptide-probes inside the PEGDAAm-co-PAA hydrogels with EDC/NHS, un-conjugated probes were removed by dialysis to prepare the FIOl (Fig. 4c). The removal of the free-peptide-probe was confirmed by measuring the absorbance of the residual peptide-probe and optical images of FIOl after dialysis (Fig. S11).

### 3.6. In vitro testing of MMP-9 detection using FIOl

The developed FIOl was reacted with 0–20 nM MMP-9 for 2.5 days at 37 °C in the dark, and, as expected, increased fluorescence intensity was observed. FIOl with 20 nM MMP-9 showed an 8.06-fold increase in fluorescence intensity, whereas FIOl with 10 and 5 nM MMP-9 showed 4.39- and 2.97-fold increases in intensities, respectively, (Fig. 4d). Drastic increases in fluorescence intensity with MMP-9 were observed after a reaction time of 2.5 days (Fig. 4f). This indicates that a specific reaction time is required for biomarker diffusion and proteolytic activity (Fig. S12). The standard deviation of FIOl under equal conditions revealed reproducible results, as shown in the overall FIOl images (Fig. S13). The LOD of FIOl was approximately 5.92 nM (Fig. S14). Besides, the selectivity of FIOl was evaluated. The selectivity of FIOl was investigated using 40 nM of MMP-3, MMP-9, and BACE1. FIOl was reacted with 0–20 nM MMP-9 for 24 h at 37 °C in the dark, and their fluorescence was measured using slit-lamp before and after the reaction. The FIOl showed increased fluorescence signals only in the presence of MMP-9, which was consistent with the selectivity data of hydrogel sensors (Fig. 4g).

Furthermore, the results show that the dual- or triple-channel of FIOl can provide the sites needed to embed reference or multiple biomarkers in the sensing hydrogel. As a proof of concept, a dual-channel of FIOl was fabricated, and an MMP-9 hydrogel sensor, as well as a FITC reference hydrogel, were attached (Fig. 4e). A comparison of the reference channel and sensing channel should give more accurate signals for quantifying biomarker levels.

### 3.7. In vivo monitoring of MMP-9 using FIOl

Next, we investigated *in vivo* diagnostic applications after confirming biocompatibility of FIOl by hemolysis test according to International Organization for Standardization (ISO) 10993-4 (ISO\_10993-4:2017, 2017) and American Society for Testing and Materials (ASTM) F756 (ASTM\_F756-17 2017) (Fig. S15). FIOl was prepared (Fig. 5a) and

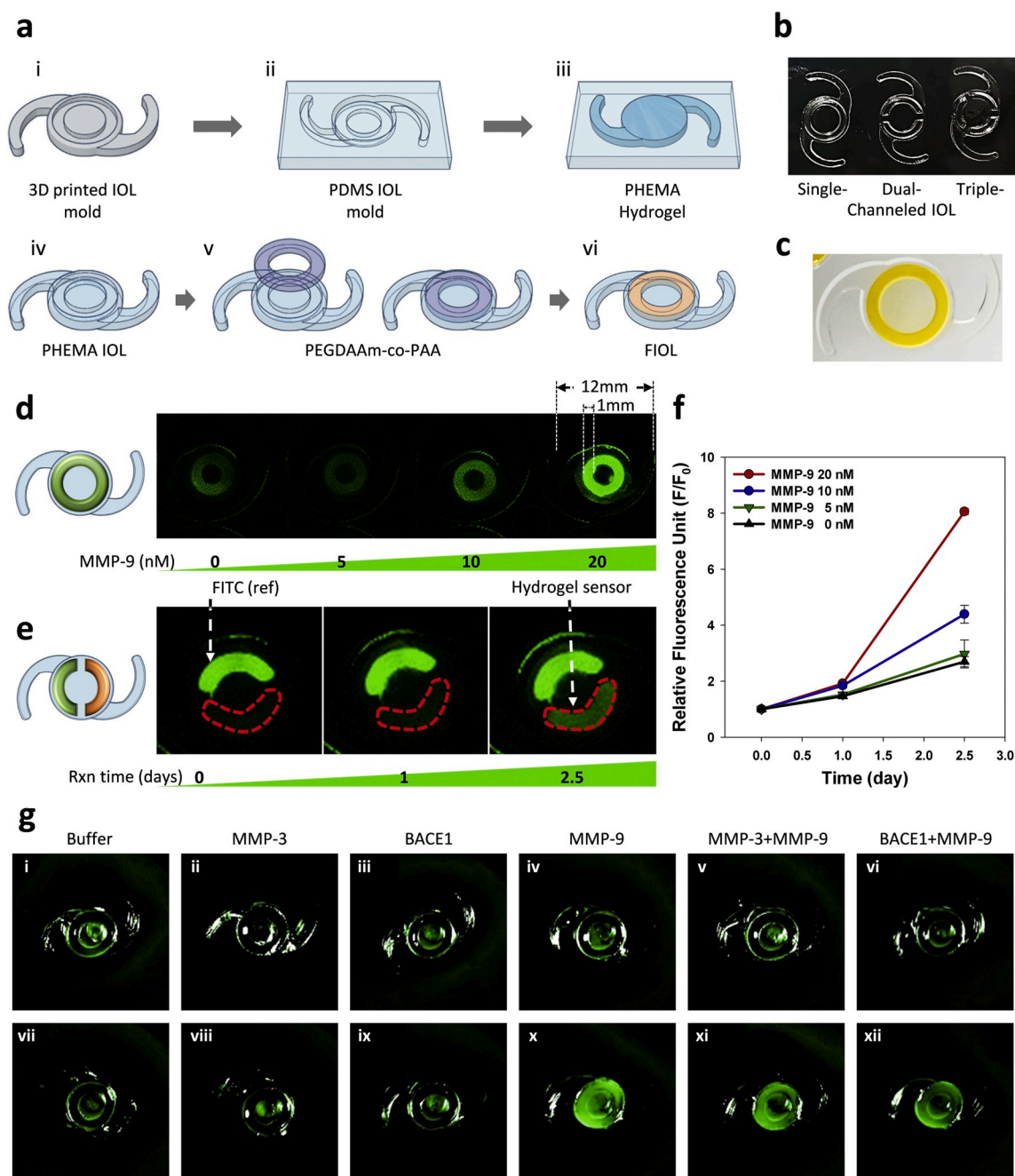


**Fig. 4.** Development of FIOI and *in vitro* testing of MMP-9 detection using FIOI. (a) Schematic illustrations of FIOI development. (i) SLA 3D-printed IOL mold followed by (ii) PDMS casting. (iii) PHEMA IOL was polymerized on PDMS mold to obtain (iv) channeled-PHEMA IOL. (v) PEGDAAm-co-PAA hydrogel was prepared in the channel of PHEMA IOL, and (vi) the peptide-probe was conjugated to obtain FIOI. (b) Images of single-, dual-, and triple-channeled-PHEMA IOL and (c) FIOI. Fluorescence images of FIOI dispersed in (d) 0–20 nM of MMP-9 after 2.5 days, and (e) time-lapse fluorescence images of dual-channeled FIOI with reference hydrogel. (f) Relative fluorescence intensity of FIOI dispersed in 0–2 nM of MMP-9 after 0, 1, and 2.5 days. Fluorescence intensity of FIOI increased over time and with increasing concentrations of MMP-9. (g) (x, xi, xii) FIOI showed fluorescence signals only in the presence of MMP-9, whereas (i, ii, iii) no signal change was observed inside the channel of FIOI without MMP-9.

implanted into the posterior chamber of the rabbit eye during cataract surgery. Specifically, the lens was removed by phacoemulsification while preserving the intact capsular bag (Fig. S16). Subsequently, FIOI was inserted using a conventional IOL injector system to minimize the corneal incision (Fig. 5b). During the IOL insertion step, FIOI was folded and loaded inside the cartridge of the injector so that the IOL-based sensing device could endure the pressure and tension during insertion. Owing to their flexibility, FIOI was advantageous for IOL insertion with smaller incisions (~2.8 mm); otherwise, a wide cornea incision would be necessary to implant the relatively rigid IOL (Movie S1). The FIOI

was stably positioned inside the posterior chamber 7 weeks post-operatively without any adverse response, including immune reactions (Fig. 5b(v)).

Supplementary data related to this article can be found at <https://doi.org/10.1016/j.bios.2020.112254>.

We next evaluated the intraocular activity of FIOI toward MMP-9. Intraocular injection of 100  $\mu$ L MMP-9 (100 nM) was given on days 0, 2, 7, 14, and 17 after post-operative day 35 (Fig. 5c). Changes in fluorescence were observed using a slit-lamp, which is frequently used in the clinical field of ophthalmology. Cobalt blue filtered light equipped in the

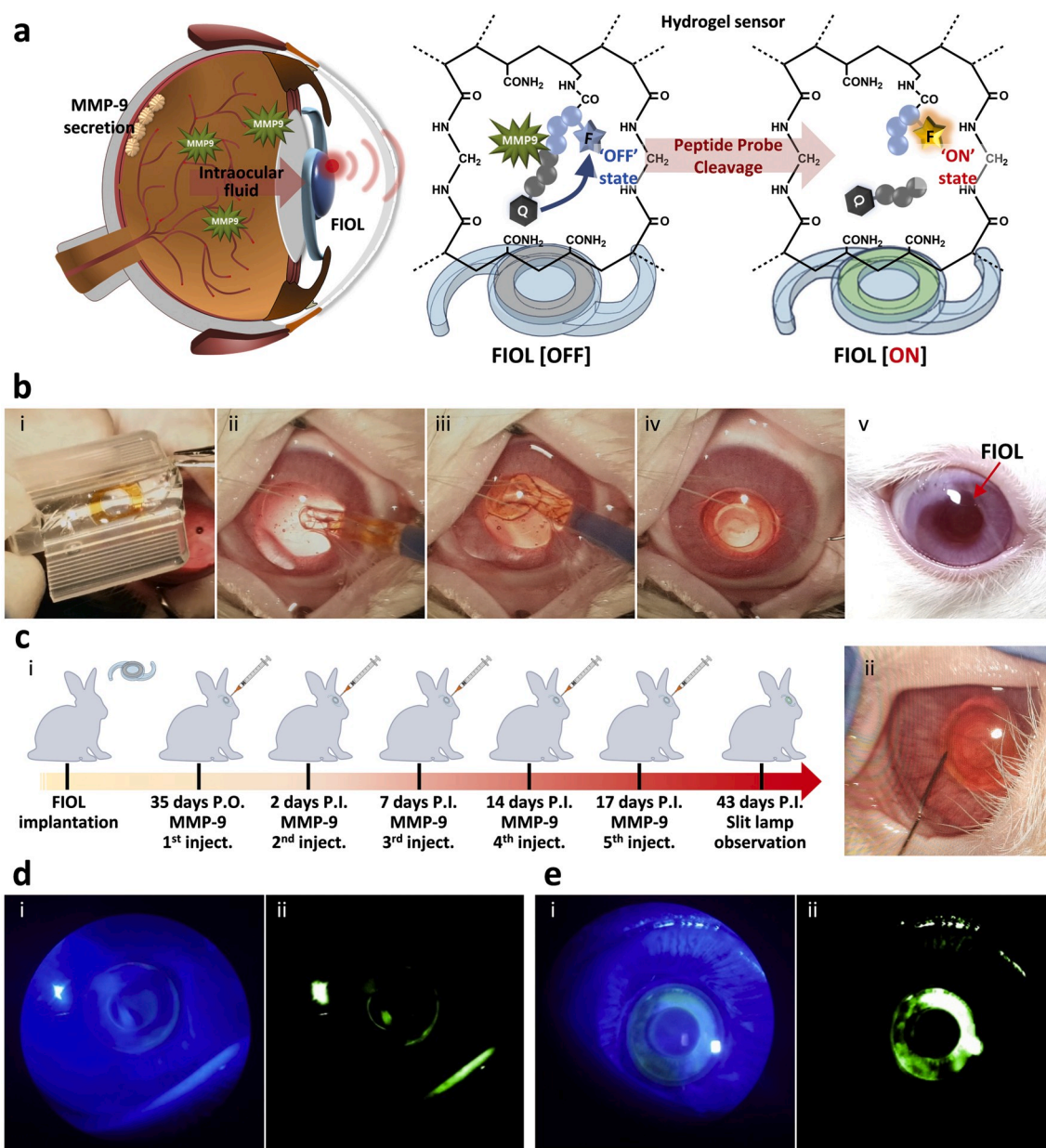


**Fig. 5.** *In vivo* monitoring of MMP-9 using FIOI. (a) Schematic illustration of the reaction mechanism of FIOI implanted inside the eye. (b) Representative photographs of the process of FIOI implantation during *in vivo* rabbit cataract surgery: i Loading of FIOI into the cartridge of the injector, (ii)–(iii) Insertion of FIOI into the posterior chamber of the eye and (iv) final implantation status of FIOI in the eye. (v) FIOI implanted in the eye maintained proper position without any adverse response, including immune reactions, over 7 weeks postoperatively. (c) (i) Schematic illustration of *in vivo* testing for MMP-9 sensing of FIOI inside the eye and (ii) representative photograph of intraocular MMP-9 injection after FIOI implantation. Slit-lamp photographs of FIOI inside the eye after (d) 2 days P.I. and (e) 43 days P.I., with (i) cobalt blue filtered light and (ii) green filtered images, respectively. (For interpretation of the references to colour in this figure legend, the reader is referred to the Web version of this article.)

slit-lamp was used to illuminate the rabbit eye; the implanted FIOI did not show green fluorescence at 2 days post-injection (P.I.) (Fig. 5d). However, a dramatically enhanced green fluorescence signal was observed at 43 days P.I., demonstrating that MMP-9 inside the eye is detectable by FIOI (Fig. 5e).

To achieve precise observation of FIOI fluorescence changes inside the eye, FIOI was implanted intraocularly to additional rabbits. MMP-9 was intraocularly injected on days 0, 3, 5, 10, and 12 after post-operative day 17. FIOI without MMP-9 injection showed no change in fluorescence (Fig. 6a); however, a dramatic increase in fluorescence was observed on the FIOI inside the MMP-9-injected rabbit eye (Fig. 6b).

In fact, we aimed to develop sustainable sensing system for diagnosis and monitoring of chronic progressive diseases like as glaucoma or

Alzheimer's disease. Such neurodegenerative diseases are slowly progressive but devastating, it is necessary to detect quiet but cumulative AH biomarkers reflecting irreversible neuropathic changes. Our FIOI-based sensing system seemed to respond slowly to injected MMP-9 into AH because MMP-9 should diffuse inside the hydrogel to cleave peptide-probe. However, since turnover rate of AH is high (approximately 2.5  $\mu\text{L}/\text{min}$ ) and FIOI constantly contacts the biomarker of AH in the eye of patients with progressive disease, it is expected that our novel FIOI system generates detectable fluorescence signal in time. Further studies using disease-specific and/or biomarker-specific animal model should be needed in the future.

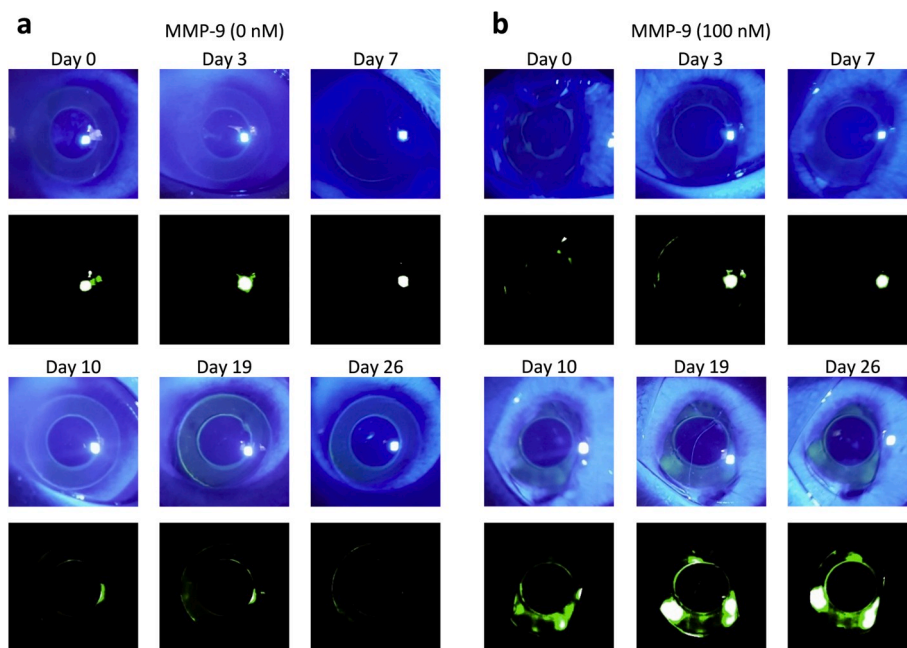


**Fig. 6.** *In vivo* monitoring of MMP-9 using FIOl. Slit-lamp photographs of *in vivo* MMP-9 sensing of FIOl inside the eye under cobalt blue filtered light. Compared to (a) FIOl without MMP-9 injection, (b) fluorescence signal of the FIOl increased after MMP-9 injection. (For interpretation of the references to colour in this figure legend, the reader is referred to the Web version of this article.)

#### 4. Conclusion

Sensitive biofluids containing prodromal biomarkers are particularly essential to detect disease-specific pathology as this occurs before clinical manifestations (Fuentes-Arderiu, 2013). In particular, it is crucial to prevent the onset or slow the progression of irreversible organ deterioration in neurodegenerative diseases as well as eye disorders (London et al., 2013; Midena et al., 2020; Tezel, 2013). AH circulating inside the eye is a promising biofluid for diagnostic LB as the eye is the only extension of the CNS that is not encased in the skull (Dehghani et al., 2018; Hillier et al., 2017; London et al., 2013; Midena et al., 2020; Tezel, 2013; van Wijngaarden et al., 2017). Furthermore, together, the blood–ocular barrier and AH bear a close resemblance to the blood–brain barrier and cerebrospinal fluid (London et al., 2013; Shah et al., 2017). AH also carries lower levels of clotting factors or confounding solubles, making it suitable for biomarker analysis (Grus et al., 2007).

The IOL is very suitable for real-time monitoring of changes of AH *in vivo*. Currently, the IOL is in high demand as the life expectancy of the aging population is increasing dramatically (Zvornicanin and Zvornicanin, 2018). According to World Health Organization Reports, the world population of people aged over 60 years will grow to 2 billion by the year 2050, which is nearly double the 900 million reported in the year 2015 (Rodriguez Manas, 2016). As the IOL, including our novel FIOl, is implanted non-invasively and semi-permanently inside the eye, its development for specific protein biomarker detection in the aging population would be advantageous.

Owing to recent advances in biosensing technology, some researchers have successfully integrated their novel monitoring sensors onto an ocular device (Araci et al., 2014; Kim et al., 2017; Narasimhan et al., 2018; Yang et al., 2018). Kim et al. reported a wearable contact lens with sensors that monitor IOP, as well as glucose, within tears on the surface of the eye (Kim et al., 2017). Additionally, intraocular implantable devices with novel sensors have been introduced by previous other studies (Araci et al., 2014; Lee et al., 2017; Narasimhan et al., 2018; Yang et al., 2018). Araci et al. demonstrated that microfluidic-based IOP sensors embedded in the IOL could be implanted to measure IOP (Araci et al., 2014). Yang et al. showed that an intraocular implantable device, not an IOL, continuously monitored glucose

concentration changes in the AH using the surface-enhanced Raman-scattering emission approach (Yang et al., 2018). However, those two novel studies used enucleated pig eyes and *ex vivo* rabbit eyes, respectively, to prove the intraocular function of their devices. Most recently, consecutive innovative studies by Lee and Narasimhan et al. reported the ability of their novel nanostructured implantable sensors to directly and accurately measure IOP (Lee et al., 2017; Narasimhan et al., 2018). These authors demonstrated the intraocular biocompatibility of their implants and the multi-functionality of the biophotonic nanostructures using rabbit eyes *in vivo*. In the present study, we not only used FDA-approved materials of FIOl but also confirmed bioactivity and biocompatibility of the FIOl through both *in vitro* and *in vivo* tests, which finally established the clinical feasibility of our novel FIOl system.

PEGDAAm hydrogel as the IOL-sensing material was advantageous owing to not only its high mechanical- and bio-stability inside the eye but also the ease of functional group modifications. As there are numerous disease-related enzymatic biomarkers, including MMP-9, our FIOl sensing system is adaptable to the detection of any biomarker, by the replacement of the peptide sequences of the fluorogenic peptide-probe with the target's specific one. In addition, biomarker detection using FIOl is advantageous for detecting cumulatively secreted biomarkers in AH. Because the FIOl can be implanted semi-permanently inside the eye, the cumulative fluorescence signal induced by early biomarkers can be recorded. Furthermore, we also found recently that the fluorescence image of FIOl can be measured using a commercially available ultra-widefield retinal imaging device (i.e., Optos® 200Tx, Optos plc, Dunfermline, Scotland), which denotes its facile applicability to general ophthalmic clinics (Fig. S17).

In summary, we developed a novel MMP-9-responsive FIOl by considering several factors. (i) PEGDAAm was selected as a biocompatible and biostable hydrogel material, showing enhanced chemical stability not only in acidic and basic buffers but also in BSS solutions. (ii) Hydrogel concentration was optimized (5 wt %) to control the mesh size to allow biomarker penetration but not to allow other cells or proteins to diffuse. (iii) A label-free detection method was adapted in IOL-based sensing devices. As a proof of concept, an MMP-9 specifically activatable peptide-probe-conjugated fluorogenic PEGDAAm-co-PAA hydrogel sensor was developed, and its LOD was analyzed (4.02 nM). Finally, (iv)

the clinical applicability of the FIOL through long-term application in live rabbit eyes was demonstrated.

In conclusion, the biostable label-free MMP-9 hydrogel sensor attached to an IOL was the first to demonstrate not only hydrogel-based macromolecular enzymatic biomarker-sensing ability but also potential clinical applications *in vivo* for long-term examination.

#### Author contributions

M.-K.S. and Y.W.J. designed the study, performed experiments, analyzed the results, and wrote the manuscript. M.-K.S., H.L., W.-S.J., J. K., and B.M. developed the materials and sensors and analyzed the data. Y.W.J., C.-E.M., and M.-K.S. performed implantation surgery and *in vitro/in vivo* tests. B.K. and M.-H.K. provided valuable suggestions and discussed the results. H.K.L. and S.H. conceived the idea and designed the study.

#### Declaration of competing interest

The authors declare that they have no known competing financial interests or personal relationships that could have appeared to influence the work reported in this paper.

#### CRediT authorship contribution statement

**Moo-Kwang Shin:** Methodology, Investigation, Formal analysis, Project administration, Writing - original draft, Writing - review & editing. **Yong Woo Ji:** Methodology, Investigation, Writing - original draft, Writing - review & editing. **Chae-Eun Moon:** Investigation, Formal analysis. **Hyo Lee:** Investigation. **Byunghoon Kang:** Resources. **Woo-Seok Jinn:** Investigation. **Jisun Ki:** Resources. **Byungeol Mun:** Investigation. **Myeong-Hoon Kim:** Resources. **Hyung Keun Lee:** Conceptualization, Supervision, Funding acquisition. **Seungjoo Haam:** Conceptualization, Supervision, Funding acquisition.

#### Acknowledgments

This work was supported by a grant from the Korea Health Technology R&D Project through the Korea Health Industry Development Institute (KHIDI), funded by the Ministry of Health & Welfare, Republic of Korea (grant number: HI18C1159), and supported by the Nano-Material Technology Development Program and the Basic Science Research Program through the National Research Foundation of Korea (NRF), funded by the Ministry of Education, Science and Technology, Republic of Korea (grant number: 2017M3A7B4041798 and 2018R1C1B6002106, respectively).

#### Appendix A. Supplementary data

Supplementary data to this article can be found online at <https://doi.org/10.1016/j.bios.2020.112254>.

#### References

- Angelova, N., Hunkeler, D., 1999. Trends Biotechnol. 17 (10), 409–421.  
 Araci, I.E., Su, B.L., Quake, S.R., Mandel, Y., 2014. Nat. Med. 20 (9), 1074–1078.  
 ASTM\_F756-17, 2017. Standard Practice for Assessment of Hemolytic Properties of Materials. ASTM International. Developed by Subcommittee F04.16.  
 Banerjee, I., Pangule, R.C., Kane, R.S., 2011. Adv. Mater. 23 (6), 690–718.  
 Benton, J.A., Fairbanks, B.D., Anseth, K.S., 2009. Biomaterials 30 (34), 6593–6603.

- Boerger, M., Funke, S., Leha, A., Roser, A.E., Wuestemann, A.K., Maass, F., Bahr, M., Grus, F., Lingor, P., 2019. Park. Relat. Disord. 63, 3–9.  
 Browning, M.B., Cereceres, S.N., Luong, P.T., Cosgriff-Hernandez, E.M., 2014. J. Biomed. Mater. Res. 102 (12), 4244–4251.  
 Browning, M.B., Cosgriff-Hernandez, E., 2012. Biomacromolecules 13 (3), 779–786.  
 Busbee, B.G., Brown, M.M., Brown, G.C., Sharma, S., 2002. Ophthalmology 109 (3), 606–612 discussion 612–603.  
 Dehghani, C., Frost, S., Jayasena, R., Masters, C.L., Kanagasigam, Y., 2018. Invest. Ophthalmol. Vis. Sci. 59 (8), 3554–3563.  
 Drury, J.L., Mooney, D.J., 2003. Biomaterials 24 (24), 4337–4351.  
 Ekker, M.S., Janssen, S., Seppi, K., Poewe, W., de Vries, N.M., Theelen, T., Nonnekes, J., Bloem, B.R., 2017. Park. Relat. Disord. 40, 1–10.  
 Elbert, D.L., Hubbell, J.A., 2001. Biomacromolecules 2 (2), 430–441.  
 Fields, G.B., Netzelarnett, S.J., Windsor, L.J., Engler, J.A., Birkedalhansen, H., Vanwart, H.E., 1990. Biochemistry 29 (28), 6670–6677.  
 Fuentes-Arderiu, X., 2013. Clin. Chem. Lab. Med. 51 (9), 1689–1690.  
 Green, A.J., McQuaid, S., Hauser, S.L., Allen, I.V., Lyness, R., 2010. Brain 133 (Pt 6), 1591–1601.  
 Grus, F.H., Joachim, S.C., Pfeiffer, N., 2007. Proteomics Clin. Appl. 1 (8), 876–888.  
 Hillier, R.J., Ojaimi, E., Wong, D.T., Mak, M.Y., Berger, A.R., Kohly, R.P., Kertes, P.J., Forooghian, F., Boyd, S.R., Eng, K., Altomare, F., Giavedoni, L.R., Nisenbaum, R., Muni, R.H., 2017. Retina 37 (4), 761–769.  
 Hoffman, A.S., 2002. Adv. Drug Deliv. Rev. 54 (1), 3–12.  
 Inoue, T., Kawaji, T., Tanihara, H., 2013. Invest. Ophthalmol. Vis. Sci. 54 (8), 5353–5358.  
 ISO\_10993-4:2017, 2017. Biological Evaluation of Medical Devices — Part 4: Selection of Tests for Interactions with Blood. International Organization for Standardization.  
 Janciauskiene, S., Westin, K., Grip, O., Krakau, T., 2011. Eur. J. Ophthalmol. 21 (1), 104–111.  
 Jonas, J.B., Tao, Y., Neumaier, M., Findeisen, P., 2012. Acta Ophthalmol. 90 (5), e381–e388.  
 Kang, G.Y., Bang, J.Y., Choi, A.J., Yoon, J., Lee, W.C., Choi, S., Yoon, S., Kim, H.C., Baek, J.H., Park, H.S., Lim, H.J., Chung, H., 2014. J. Proteome Res. 13 (2), 581–595.  
 Kersten, E., Paun, C.C., Schellevis, R.L., Hoyng, C.B., Delcourt, C., Lengyel, I., Peto, T., Ueffing, M., Klaver, C.C.W., Dammeier, S., den Hollander, A.I., de Jong, E.K., 2018. Surv. Ophthalmol. 63 (1), 9–39.  
 Kim, J., Kim, M., Lee, M.S., Kim, K., Ji, S., Kim, Y.T., Park, J., Na, K., Bae, K.H., Kim, H. K., Bien, F., Lee, C.Y., Park, J.U., 2017. Nat. Commun. 8.  
 Kohnen, T., 2018. J. Cataract Refract. Surg. 44 (2), 121–123.  
 Lambert, N.G., ElShelmani, H., Singh, M.K., Mansergh, F.C., Wride, M.A., Padilla, M., Keegan, D., Hogg, R.E., Ambati, B.K., 2016. Prog. Retin. Eye Res. 54, 64–102.  
 Lee, J.O., Park, H., Du, J., Balakrishna, A., Chen, O., Sretavan, D., Choo, H., 2017. Microsyst. Nanoeng 3, 17057.  
 Li, S., Jie, Y., 2019. Curr. Opin. Ophthalmol. 30 (1), 39–43.  
 Lim, J.K., Li, Q.X., He, Z., Vingrys, A.J., Wong, V.H., Currier, N., Mullen, J., Bui, B.V., Nguyen, C.T., 2016. Front. Neurosci. 10, 536.  
 London, A., Benhar, I., Schwartz, M., 2013. Nat. Rev. Neurosci. 9 (1), 44–53.  
 Mahou, R., Wandrey, C., 2012. Polymers 4 (1), 561–589.  
 Midena, E., Bini, S., Martini, F., Enrica, C., Pilotto, E., Micera, A., Esposito, G., Vujosevic, S., 2020. Retina 40 (1), 126–134.  
 Narasimhan, V., Siddique, R.H., Lee, J.O., Kumar, S., Ndjamen, B., Du, J., Hong, N., Sretavan, D., Choo, H., 2018. Nat. Nanotechnol. 13 (6), 512–+.  
 Park, S.J., Lee, J.H., Kang, S.W., Hyon, J.Y., Park, K.H., 2016. J. Kor. Med. Sci. 31 (6), 963–971.  
 Pietrowska, K., Dmuchowska, D.A., Krasnicki, P., Mariak, Z., Kretowski, A., Ciborowski, M., 2018. J. Pharmaceut. Biomed. Anal. 159, 23–36.  
 Rodriguez Manas, L., 2016. Rev. Esp. Geriatr. Gerontol. 51 (5), 249–251.  
 Seo, S., Lee, J., Kwon, M.S., Seo, D., Kim, J., 2015. ACS Appl. Mater. Interfaces 7 (36), 20342–20348.  
 Shah, T.M., Gupta, S.M., Chatterjee, P., Campbell, M., Martins, R.N., 2017. Mol. Psychiatr. 22 (3), 353–363.  
 Stevens, K.R., Miller, J.S., Blakely, B.L., Chen, C.S., Bhatia, S.N., 2015. J. Biomed. Mater. Res. 103 (10), 3331–3338.  
 Tamhane, M., Cabrera-Ghayouri, S., Abelian, G., Viswanath, V., 2019. Pharm. Res. (N. Y.) 36 (3), 40.  
 Tezel, G., 2013. Prog. Retin. Eye Res. 35, 18–43.  
 Ulijn, R.V., Bibi, N., Jayawarna, V., Thornton, P.D., Todd, S.J., Mart, R.J., Smith, A.M., Gough, J.E., 2007. Mater. Today 10 (4), 40–48.  
 Vafadari, B., Salamian, A., Kaczmarek, L., 2016. J. Neurochem. 139 (Suppl. 2), 91–114.  
 van Wijngaarden, P., Hadoux, X., Alwan, M., Keel, S., Dirani, M., 2017. Clin. Exp. Ophthalmol. 45 (1), 54–61.  
 Wahid Khan, E.M., Jaffe, Michael, Domb, Abraham J., 2014. Focal Controlled Drug Delivery (Illinois).  
 Yang, D., Afrosheh, S., Lee, J.O., Cho, H., Kumar, S., Siddique, R.H., Narasimhan, V., Yoon, Y.Z., Zayak, A.T., Choo, H., 2018. Anal. Chem. 90 (24), 14269–14278.  
 Zvornicanin, J., Zvornicanin, E., 2018. J. Curr. Ophthalmol. 30 (4), 287–296.